JTAM (Jurnal Teori dan Aplikasi Matematika)
http://journal.ummat.ac.id/index.php/jtam
p-ISSN 2597-7512 | e-ISSN 2614-1175
Vol. 9, No. 3, July 2025, pp. 1053-1067

A Spatiotemporal Analysis of Humidity Pattern in Bali using Space-Time Kriging with Seasonal Drift

Salma Fitri Nugroho[1*], Rahma Fitriani[1], Atiek Iriany[1]
[1]Department of Statistics, Universitas Brawijaya, Indonesia
salma_f@student.ub.ac.id

Article History:
Received : 28-04-2025
Revised : 27-05-2025
Accepted : 28-05-2025
Online : 05-07-2025

Keywords:
Humidity;
Interpolation;
Kriging;
Space-time.

ABSTRACT

Climate plays a vital role in framing the characteristics of tourist activity. Humidity reflects the amount of moisture in the air relative to the maximum it can hold at a specific temperature, it has a direct influences on perceived comfort levels. Bali, one of the most popular destinations renowned for its breathtaking natural beauty and varied landscapes. However, this island is currently served by only four climate observation stations which are insufficient to capture the humidity across the island. Therefore, this research aims to model humidity levels in Bali based on four observed locations at 2019-2023 using the space-time kriging with seasonal drift and predict humidity at unobserved locations. This approach was choosen due to the strong seasonal pattern exhibited in climate data, which leading to non-stationary. The space-time kriging method is applied to the residuals. The most effective model identified was the exponential-exponential-Gaussian (Exp-Exp-Gau) model using a sum-metric structure. This model provided the lowest RMSE of 2.1442. Humidity contour maps suggest a gradual decline in humidity levels over time across Bali. This trend may have significant impacts for both environmental quality and the tourism sector. Lower humidity levels could lead to increased discomfort for tourists and potentially reduce the attractiveness of the destination. Theoretically, the development of the kriging model enhances the accuracy of predictions, as shows by the low RMSE. Practically, these findings emphasize the importance of integrating climate considerations into sustainable tourism planning and management strategies based on the humidity information.

Crossref
https://doi.org/10.31764/jtam.v9i3.30874

A. INTRODUCTION

Bali island, one of the most popular destinations due to its breathtaking natural beauty and varied landscapes (Ramadhani et al., 2024). This island is also notable for its relaxing beaches, which are perfectly suited for a water sport activity. In addition, Bali features a warm tropical climate that attracts international tourist because of the warm temperatures and sunshine throughout the year (Susanto et al., 2020). Bali has two main seasons; the dry season, which occurs from May to October, and the wet season, from November to April (Ananta et al., 2024). The prevailing weather conditions enhance Bali's allure and contribute to the timing and nature of tourist visits (Zeng et al., 2023).

Climate plays an important role in influencing tourist visit with pleasant weather during the dry season encourages higher visitor numbers, whereas the wet season may lead to decline in tourism-related activities patterns (Atasoy & Guneysu Atasoy, 2020). The interdependence between climate and tourism highlight how weather conditions can directly and indirectly affect economic performance and human activities in the region (Simorangkir et al., 2024).

Several climatic variables influence comfort conditions for tourist with the one of the most effective and applicable thermal indicators, known as the Tourist Climate Index (TCI) (Lukić et al., 2021). This index measures tourist comfort based on various weather parameters, such as humidity level, air temperature, precipitation, wind speed and sunshine hours. Temperature and humidity are the variables that most influence the TCI (Jong et al., 2024). Humidity reflects the amount of moisture in the air relative to the maximum it can hold at a specific temperature (Mondal et al., 2025). High humidity can lead to increased precipitation, which affects tourist comfort (Zeiss et al., 2022). Furthermore, humidity patterns can predict weather changes, with high humidity make it feel hotter and low humidity contributing to a drier atmosphere (Baldwin et al., 2023).

Several previous studies have focused on interpolating and predicting climate indicators using various methodologies, such as ordinary kriging (Taharin & Roslee, 2021), inverse distance weighted (Amelia et al., 2023), SARIMA (Liu, 2024), ARIMA and remote sensing (Zaharieva et al., 2025). However, these studies often focus only on either the geographic location or temporal aspect. Climate data possess a space-time data type that relates both space and time dimension. Therefore, the information derived from space-time data essential. Kriging is a statistical technique used to estimate values at unmeasured locations by using information from measured locations (Adhikary et al., 2017). It accounts for the space variability of data by utilizing a semivariogram function, which illustrates the relationship between values at different locations. However, selecting an appropriate semivariogram model and a kriging method that align with underlying assumptions poses challenges (Lv & Du, 2021). There are three different kriging method that can be used, such as simple kriging (Ro & Yoo, 2022), ordinary kriging and universal kriging (Khan et al., 2023).

Space-time kriging extends the basic kriging method by considering not only geographic location but also the time aspect of the data (Du et al., 2018). This method is capable to capture dynamic changes over time (Dhaher & Shexo, 2023). Space-time kriging conducts interpolation by leveraging spatiotemporal autocorrelation among dispersed values to predict values at unobserved locations. This method applies weights to spatiotemporal data from observed points and provides prediction variance to indicate the accuracy of these predictions (Ding et al., 2024). Climate data often exhibit seasonal drift, which make it non-stationary (Krock et al., 2022). To remove the seasonal component from the data, time-series decomposition can be applied. While decomposition removes only the seasonal component, the residual may still contain location and time trends. Space-time regression kriging can be employed to interpolate non-stationary data, as this method considers both location and time trends (Du et al., 2018).

This research aims to model humidity in Bali using space-time kriging with seasonal drift to predict humidity at unobserved locations. The result of this prediction will not only enhance the understanding of humidity patterns but also serve as valuable resource for policymakers and stakeholders in the tourism industry, especially in Bali. Furthermore, the insights gained from this research can aid in the development of sustainable tourism strategies that consider seasonal variations in climate.

B. METHODS

1. Data and Research Variables

The data is provided by the Bali Province BMKG (Badan Meteorologi Klimatologi dan Geofisika), which contains an average percentage of humidity data for Bali. Humidity selected because of its big contribution for TCI value. The data were obtained for four stations: Sanglah Geophysics Station in Denpasar, Negara Climatology Station in Jembrana, Kahang-kahang Geophysics Station in Karangasem, and Ngurah Rai Meteorology Station in Badung. Humidity was recorded monthly over five years, from January 2019 to December 2023.

2. Time Series Decomposition

The analysis was conducted after processing humidity data into space-time data type formats using RStudio software. There are four steps of the analysis process. The first step is processing the original data to satisfy stationarity by using time series decomposition to remove the seasonal component for each location. This step performed because seasonality in climatic data is obvious and that is the main factor that makes the data non-stationary. The different stations exhibit different seasonality patterns, which can be described by Equation (1) (Das & Barman, 2025).

$$Z(s,t) = Se(s,t) + R(s,t) \tag{1}$$

where Z represents the space-time data of humidity at location s and time t which indicates the number of a month ($t = 1, \dots, 60$). The Z comprises two components, $Se(s,t)$ as a space-time seasonal component and $R(s,t)$ is the residual from removed seasonal component.

3. Regression Analysis

The second step involves modeling space-time regression to remove the trend of location and time. The location trend variables included the coordinates (x,y) or (longitude, latitude), while the time trend variable consists the month of the research. The relationship between these various trend variables can be represented by the space-time regression model as shown in Equation (2) (Li et al., 2020).

$$R(s,t) = \sum_{i=0}^{p} \beta_i f_i(s,t) + \varepsilon_i(s,t) \tag{2}$$

where R represents the seasonality-removed data, comprising $p + 1$ components. The p denotes the number of regression variables (in this research, $p = 3$ corresponds to longitude, latitude and month of the year). The β_i represent as a coefficient of regression and $f_i(s,t)$ are the known variables over the space-time domain. Specifically, $k_0 f_0(s,t)$ represents the intercept of the model, while $\varepsilon_i(s,t)$ denotes the residual of the regression.

4. Empirical Semivariogram

Conceptually, the residuals of the regression still contain space-time information, assuming that the residuals of the regression $\varepsilon_i(s,t)$ are stationary. Thus, the third step is modeling the residuals $\varepsilon_i(s,t)$ using a space-time semivariogram, A space-time semivariogram is used to describe spatial dependence in regionalized variable and time dependence in time lags. There are two types of semivariogram, the empirical space-time semivariogram which is calculated using the sampled data and the theoretical space-time semivariogram. The empirical space-time semivariogram function is calculated using Equation (3) (Venkatachalam & Kumar, 2017).

$$\gamma_{st}(\boldsymbol{u},\boldsymbol{v}) = \frac{1}{2}V(\varepsilon(\boldsymbol{s}+\boldsymbol{u},t+v) - \varepsilon(\boldsymbol{s},t)) \tag{3}$$

where, u defines space distance and v defines time lag. After constructing the empirical space-time semivariogram, fitting a theoretical space-time semivariogram with an appropriate curve shape by comparing several components of the semivariogram such as nugget effect, sill, and range.

5. Theoretical Semivariogram

In this research, the space and time marginal semivariograms will be modeled using the exponential model and the Gaussian model, expressed in Equation (4) and (5), respectively.

$$\gamma(u) = c_0 + c\left[1 - \exp\left(-\frac{u}{a}\right)\right] \tag{4}$$

$$\gamma(u) = c_0 + c\left[1 - \exp\left(-\frac{u^2}{a^2}\right)\right] \tag{5}$$

where, c_0 represents the nugget, u represents the distance in either space or time, c signifies the partial sill, and a indicates the effective range.

After determining the semivariogram model for both space and time, the next step is modeling the space-time semivariogram, which can illustrate the structure of space-time data dependence. Several methods can be used to model space-time semivariogram, including the metric model (Zhao et al., 2020), the separable model (Lambardi Di San Miniato et al., 2022), the sum-metric model (O'Rourke & Kelly, 2015), and the sum-product model (Bachrudin et al., 2023). In this research, the sum-metric model will be employed due to its flexibility in modeling the residuals of the regression $\varepsilon_i(s,t)$, as shown in Equation (6).

$$\gamma_{st}(\boldsymbol{u},\boldsymbol{v}) = \gamma_{st}(\boldsymbol{u},\boldsymbol{0}) + \gamma_{st}(\boldsymbol{0},\boldsymbol{v}) + \gamma_{st}\sqrt{||u||^2 + (k.|v|)^2} \tag{6}$$

to determine the best model in this research, a comparison will be conducted using the RMSE as expressed in Equation (7) (Rahmawati, 2020).

$$RMSE = \sqrt{\frac{1}{\#N(\boldsymbol{h},u)} \sum_{i=1}^{N(\boldsymbol{h},u)} \left(\hat{\gamma}(\boldsymbol{h},u) - \gamma(\boldsymbol{h},u)\right)^2} \tag{7}$$

6. Space-Time Kriging with Seasonal Drift

The final step is carried out space-time prediction of the residual values for all locations. The prediction is performed using ordinary space-time kriging, which represent as Equation (8).

$$\varepsilon^*(\boldsymbol{s_0}, t_0) = \sum_{i=1}^{n} \lambda_i\, \varepsilon(\boldsymbol{s_i}, t_i) \tag{8}$$

where $\varepsilon(\boldsymbol{s_i}, t_i)$ is the residuals of sampled location and λ_i denotes the weights for space-time kriging, as shown in Equation (9).

$$\begin{pmatrix} \gamma(\boldsymbol{s}_1 - \boldsymbol{s}_1, t_1 - t_1) & \cdots & \gamma(\boldsymbol{s}_1 - \boldsymbol{s}_n, t_1 - t_n) & 1 \\ \vdots & \ddots & \vdots & \vdots \\ \gamma(\boldsymbol{s}_n - \boldsymbol{s}_1, t_1 - t_1) & \cdots & \gamma(\boldsymbol{s}_n - \boldsymbol{s}_n, t_n - t_n) & 1 \\ 1 & \cdots & 1 & 0 \end{pmatrix} \begin{pmatrix} \lambda_1 \\ \vdots \\ \lambda_n \\ \alpha \end{pmatrix} = \begin{pmatrix} \gamma(\boldsymbol{s}_1 - \boldsymbol{s}_0, t_1 - t_0) \\ \vdots \\ \gamma(\boldsymbol{s}_n - \boldsymbol{s}_0, t_n - t_0) \\ 1 \end{pmatrix} \tag{9}$$

The space-time regression kriging with seasonal drift estimation is given by Equation (10).

$$\hat{Z}_{(s_0,t_0)} = Se(s_0, t_0) + \sum_{i=0}^{p} k_i f_i(s,t) + \varepsilon^*(\boldsymbol{s_0}, t_0) \tag{10}$$

C. RESULT AND DISCUSSION

1. Data Exploration

The time series plots illustrated in Figure 1 show the humidity conditions recorded across four different stations (Sanglah, Negara, Kahang-Kahang, and Ngurah Rai) from 2019 to 2023. An obvious seasonality pattern is evident, especially at the Kahang-Kahang station. It indicates similar humidity conditions throughout the year. The Sanglah station exhibit relatively stable humidity level around 75-80% with only minor seasonal fluctuations observed.

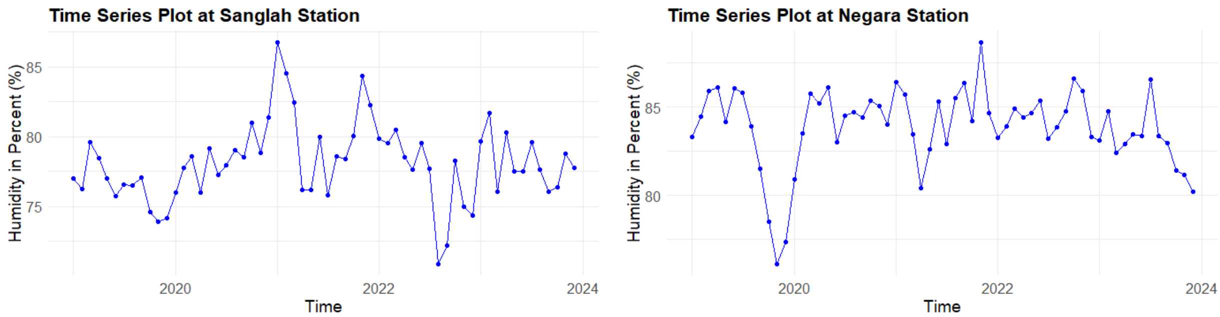

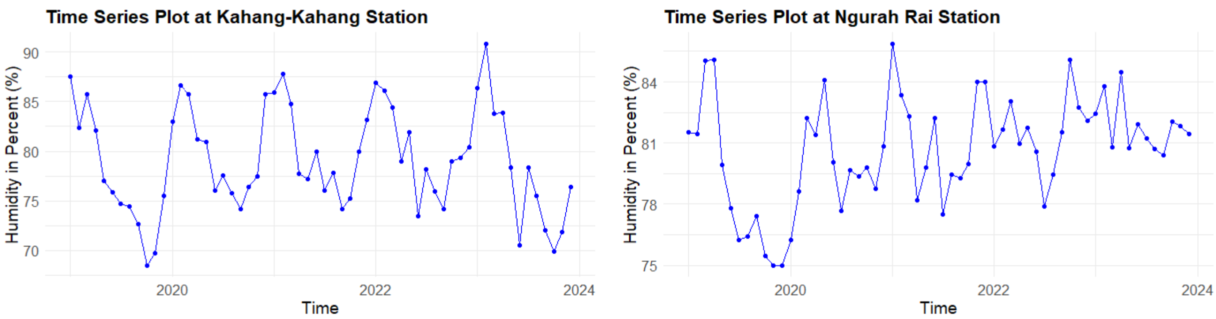

Figure 1. Time series plot in each station

In contrast, the Negara station shows a slight upward trend and recorded the humidity level is around 80-85%, which is notably higher than Sanglah station. Both Kahang-Kahang and Ngurah Rai stations indicate the strong seasonal effects that characterized by significant variations between wet and dry seasons. These seasonal changes contribute to extreme fluctuations in humidity levels emphasizing the dynamic nature of the climate in these regions. Figure 2 and Figure 3 show scatter plots of the relationship between humidity and location coordinate (longitude and latitude) for several different months that randomly selected. In most months, there are no distinct linear trend of location coordinates and humidity level. However, some months like May 2021, August 2021 and September 2022 show relatively lower humidity at higher longitudes.

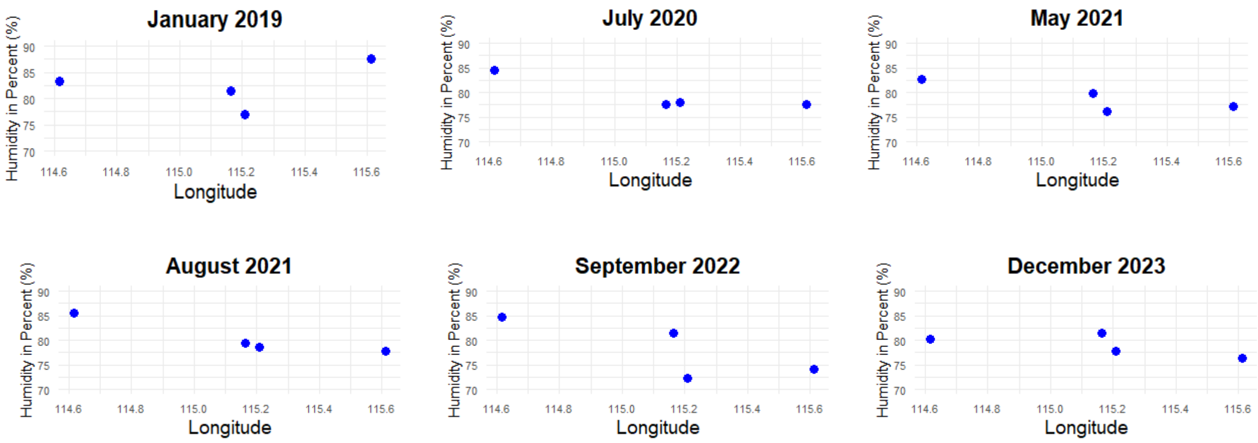

Figure 2. Longitude trend in several time

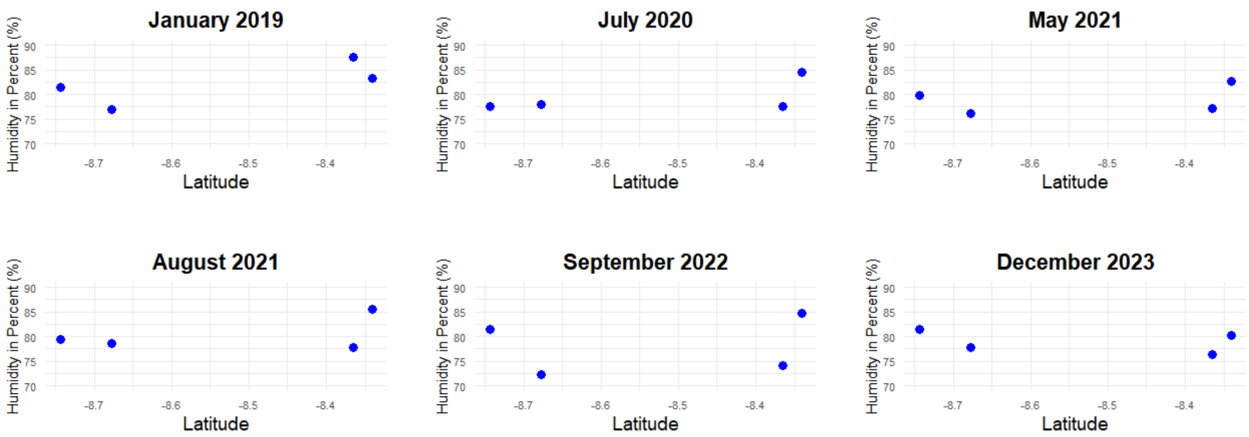

Figure 3. Latitude trend in several time

Conversely, in, July 2020, the humidity tends to be higher across most latitudes. This exploration suggest that latitude and longitude do not exhibit a strong trend concerning humidity, but still contain a location trend in several time. Thus suggestion remains an underlying spatial pattern that influences the choise of kriging method employed in the analysis. Before applying the kriging method, it is important to first address any space and time trends present in the data. Both space and time trends might be impacted to kriging result remining the underlying assumption of the kriging itself. A time series decomposition is employed as a step to removed the obvious seasonality patterns into a SAD (seasonality Adjusted Data). After removing the seasonal pattern, a regression analysis is carried out as a preliminary step to identify and remove location trends.

2. Time Series Decomposition

The removal of seasonal component is needed to eliminate the time trend, as climatic data is often characterized by seasonal patterns. This process is conducted to enhance the accuracy of interpolation. Seasonal removal is applied to each station location, given that each location may have the different seasonality pattern. It is conducted using additive time series decomposition which is simpler than other methods. Figure 4 shows the time series decomposition plot using the additive method using Equaton (1).

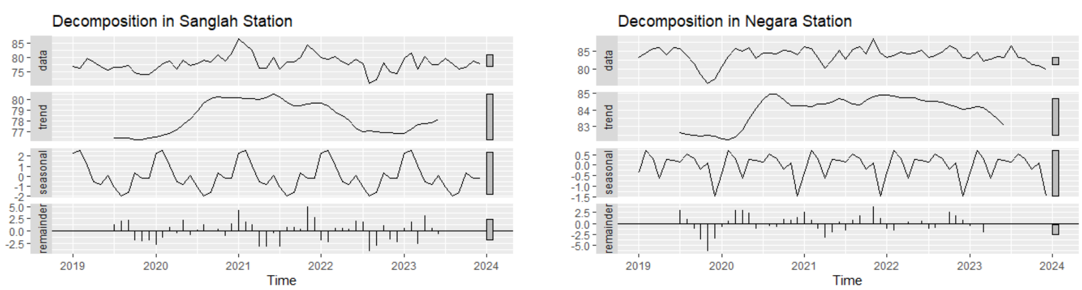

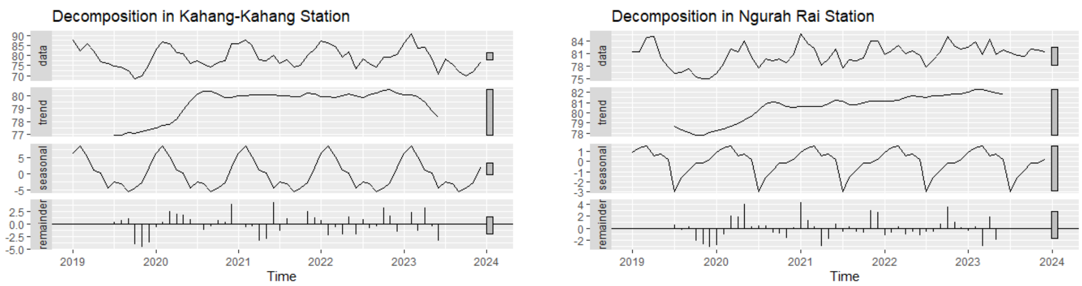

Figure 4. Decomposition plot in each station

Figure 4 shows the seasonal components derived from each location exhibit a clear annual cycle, which aligns well with the monthly data used in this research. This observation indicates a strong seasonal influence on humidity, likely tied to wet and dry seasons in the region. Furthermore, it is notable that the estimated seasonal components remain relatively stable over time, suggesting that the underlying climatic patterns are consistent across the observed period. This stability enhances the reliability of the seasonal components as indicators of humidity variation. The specific seasonal components from Equation (1) for each station are detailed in Table 1.

Table 1. Seasonal component for each station

	Jan	Feb	Mar	Apr	May	Jun	Jul	Aug	Sep	Oct	Nov	Dec
Sanglah	2.308	2.557	1.079	-0.57	-0.76	0.099	-1.09	-1.93	-1.64	0.309	-0.18	-0.19
Negara	-0.37	0.692	0.331	-0.61	0.291	0.248	0.140	0.528	0.306	-0.21	0.104	-1.46
Kahang-Kahang	6.222	8.472	5.298	1.106	0.199	-4.43	-2.58	-3.27	-5.54	-4.58	-2.77	1.875
Ngurah Rai	0.962	1.369	1.538	0.606	0.781	0.262	-2.95	-1.57	-0.89	-0.17	-0.12	0.180

After decomposition, the data will be reduced by the seasonal component. This step is conducted because seasonal variation not aligns with the underlying assumption of space-time ordinary kriging. The data with seasonal component removed is referred to as seasonality-adjusted data (SAD).

3. Trend Regression

The seasonality-adjusted data (SAD) still exhibit a trend that captures variability across both space and time dimension. This trend could be influenced by the space dependent covariates, such as longitude and latitude, as well as time dependent covariate, specifically the month of observed data. To know the relationship between these covariates, a multiple linear regression analysis is conducted using the all-subsets regression method. This approach allows to explore various combination of covariates to identify the significant predictors of the observed trends, The parameter estimation of multiple linier regression model in Equation (2) are detailed in Table 2.

Table 2. Parameter estimation of regression analysis

Parameter	Estimation	SE	t value	p-value	R^2	p-value
β_0 (intercept)	679.5614	55.1908	12.313	<2e-16	0.3662	<2e-16
β_1 (longitude)	-4.8999	0.4843	-10.118	<2e-16		
β_2 (latitude)	4.0672	0.9494	-4.284	2.67e-05		
β_3 (month)	-0.0319	0.0491	-0.652	0.515		

Table 2 indicates that the SAD exhibit an obvious spatial trend. This is indicated by the p-value for longitude and latitude which are lower than the alpha level of 0.05, signifying that these spatial covariates significantly influence the SAD. The negative coefficient for longitude indicates that as one moves eastward across Bali, humidity levels tend to decrease significantly. This spatial gradient may relate to Bali's topography and prevailing wind patterns. The western parts of Bali experience higher humidity since this area close to the Indian Ocean and influenced by moist oceanic air masses. While the positive latitude coefficient suggests that moving northward within Bali correlates with increasing humidity. Conversely, there is no evidence of a temporal trend as the p-value for the month exceeds the alpha level. This lack of significance may be causes by seasonality removal that obtained before. For this case, we can conclude that the seasonality component removal is effective in eliminating the time trend from origin data. The all-subsets regression model explains 36.62% of the variance in the SAD values.

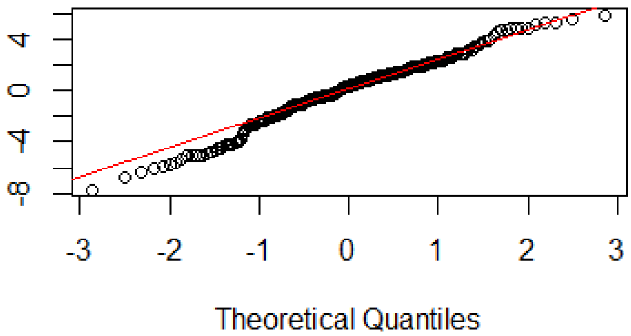

Figure 5. QQ Plot for normality test

The regression analysis residuals form a zero-mean process that preserves important space-time information. To assess the reliability of the model, normality hypothesis test was performed as shown in Figure 5. The QQ plot shows that the most of the residuals closely follow the red line. The distribution of the residuals suggests a normal distribution. Therefore, the plot indicates that the all-subsets regression model offers a good fit for the SAD values.

4. Empirical Semivariogram

Figure 6 represent the relationship between time lag (in days) and distance (in kilometers) using a color gradient that indicate the semivariance values based on Equation (3). Yellow color indicates higher semivariance, while purple indicates lower semivariance. As spatial distance increases, the semivariance value initially rise, suggesting that spatial dependence exists over shorter distances. However, beyond a certain distance, the semivariance values tend to stabilize, indicating a reduced influence of distance on the variability of the data over time.

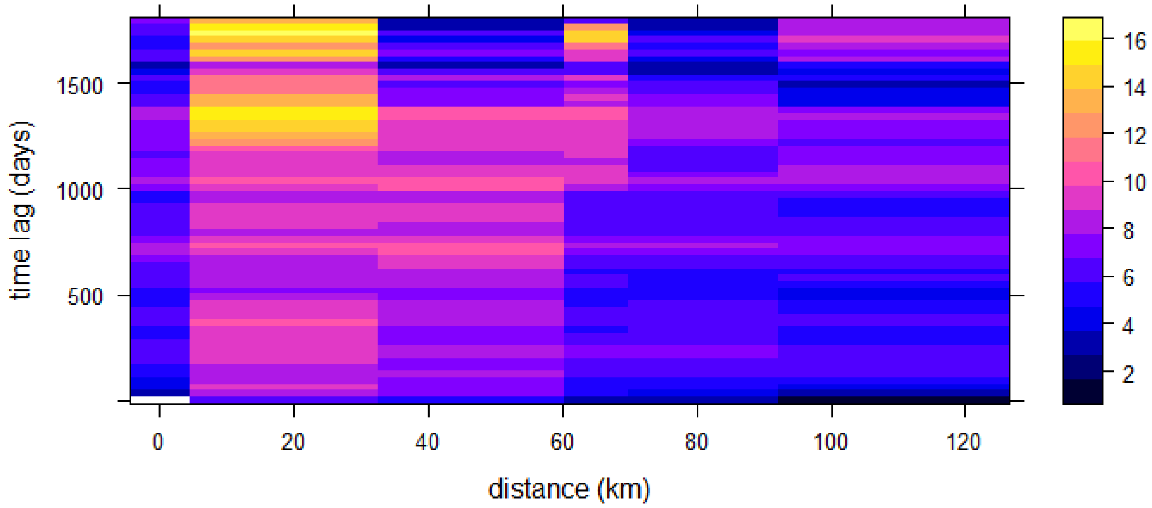

Figure 6. Empirical semivariogram

Based on the Figure 6, assumed that the semivariance stabilizes at distance of around 80 kilometers. Beyond this point, the semivariance values remain relatively constant, indicating that spatial dependence decreases significantly. In essence, once the distance reach 80 kilometers, further increases in distance do not significantly affect the variability of the data. In terms of the time aspect, the range is estimated to occurs around a time lag of 60 days. It indicates the time lag over the temporal correlation persists. Beyond this duration, the influence of time on the similarity between observations becomes minimal.

Additionally, the nugget value is assumed to be around 2, which represents the semivariance value at a distance of zero. This value typically accounts for measurement error or microscale variation. The sill also can be approximated by identifying the maximum observed semivariance in the plot. It appears that the highest values in the yellow range, likely around 16. This value indicates the point where the spatial correlation between data points has significantly decreased and the variability become relatively consistent across distances.

5. Theoretical Semivariogram

The parameter values for sill, range and nugget from the empirical space-time semivariogram serve as the foundation for fitting a theoretical space-time semivariogram model. A comparison of RMSE values based on Equation (7) for different model combination is presented in Table 3. Among all combinations, the model employing an Exponential structure for both space and time components which combined with a Gaussian joint model produced the lowest RMSE value of 2.1442. This indicates the best fit to the empirical semivariogram. This result suggests that the Exp-Exp-Gau model is the most appropriate combination for capturing the underlying space-time dependencies in the residual data.

Table 3. Comparison of RMSE for fitting theoretical semivariogram model

Space model	Time model	Joint model	RMSE
Exp	Exp	Exp	2.1445
Exp	**Exp**	**Gau**	**2.1442**
Exp	Gau	Exp	2.1564
Exp	Gau	Gau	2.1534
Gau	Exp	Exp	2.1446
Gau	Exp	Gau	2.1456

The space-time semivariogram, both empirical and theoretical served in Figure 7.

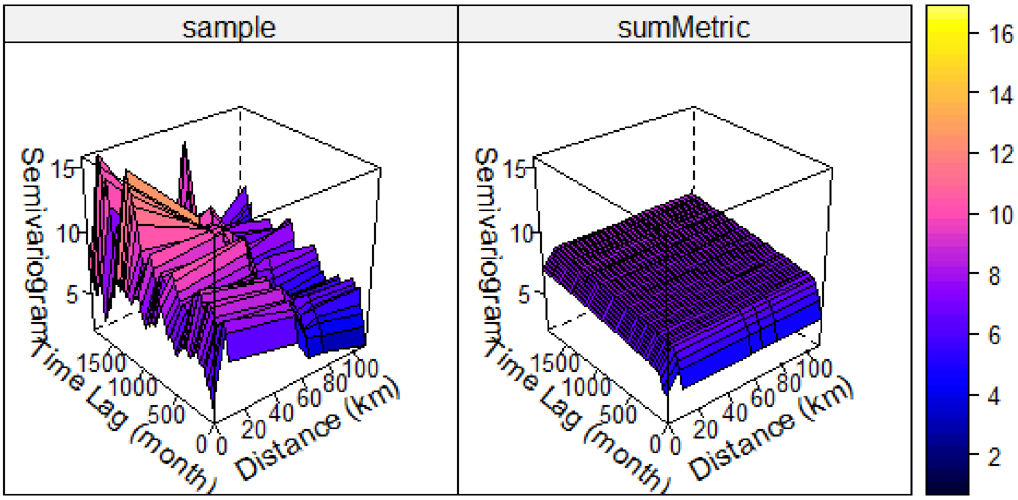

Figure 7. Space-time semivariogram; empirical semivariogram (left) and theoretical semivariogram (right)

On the left side is the empirical semivariogram, which characterized by irregular and sharp peaks. The fluctuation across the surface suggests the presence of significant space-time interaction within the data. Moreover, the theoretical space-time semivariogram shown on the right side is derived using Exp-Exp-Gau sum-metric model. This plot shows a smoother and more continuous surface reflecting the fitted values obtained from the selected theoretical model. Moreover, the joint space-time component is modelled using a Gaussian model that contributing a partial sill of 1.72 and a range of 8020.25 km. This selection of a Gaussian joint model aligns well with the smoother appearance of the theoretical semivariogram surface. Additionally, the estimated space-time anisotropy (stAni) value of approximately 102.19. This implies that a unit increase in time (one month) corresponds spatially to a change equivalent to 102.92 kilometers. In other words, temporal changes translate into spatial changes at this ratio highlight the interconnected nature of space and time in influencing the variable dynamics.

6. Space-Time Regression Kriging with Seasonal Drift

After interpolating the residual data using the kriging approach, the kriging value were combined with the regression estimations as Equation (10). This integration produced the space-time regression kriging with seasonal adjustment. The last step involved reintroducing the seasonal component base on the nearest observation location to each prediction point. The final estimates which incorporate both space and time trends and seasonal variability are presented in Figure 8.

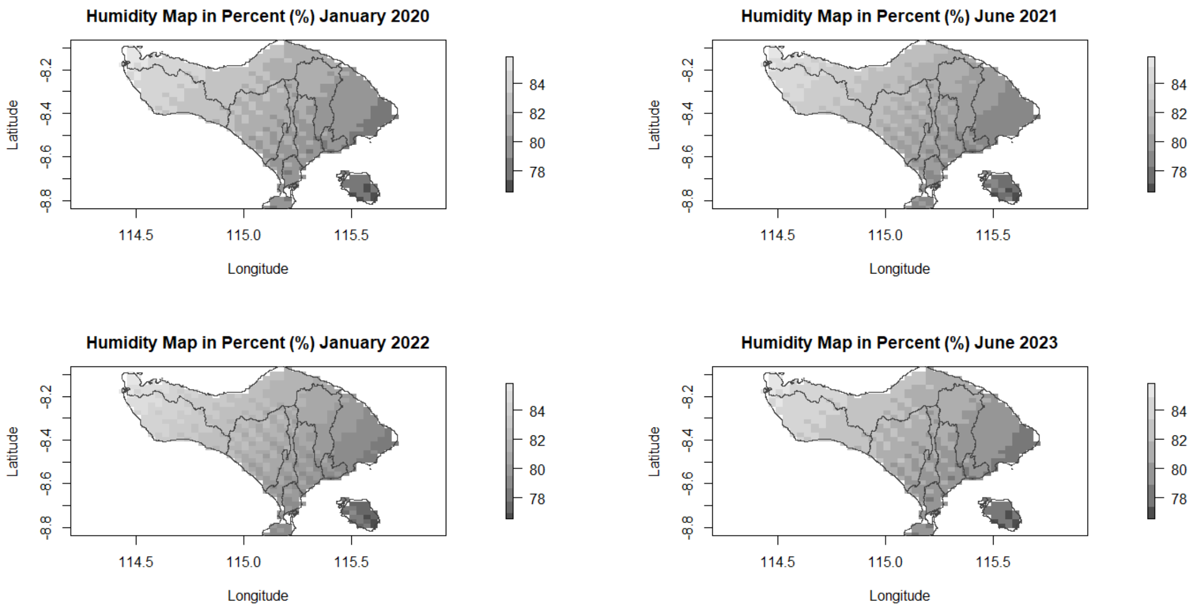

Figure 8. Contour map of integrated space-time regression kriging with seasonal drift estimation

Based on the space-time predictions, humidity levels in Bali range from approximately 70.82% to 90.90%. It can be concluded from the figure that humidity tends to increase slowly toward the western part of the research area. This spatial gradient suggests a consistent westward increase in humidity levels, likely influenced by regional climatic and geographic factors. In terms of latitude, there does not appear to be a clear trend. These findings align with the study by Toersilowati et al. (2022), which stated that the northern part of Bali experiences drier humidity conditions, while some areas in the south exhibit higher humidity.

D. CONCLUSION AND SUGGESTIONS

This research aims to analyze and predict monthly humidity levels in Bali. The results show its effectiveness provides the lowest RMSE value of 2.1442, which highlights its prediction accuracy. The map reveals that humidity levels in Bali are projected to decrease which can affect both the environmental quality and the tourism industry. Dry air conditions may lead to discomfort for tourists and reducing the appeal of the destination. Therefore, integrating climate considerations into sustainable tourism planning is crucial to mitigate these potential impacts. However, this research has certain limitations, especially regarding the limited availability of observed data which may reduce the reliability of the predictions. Sparse of distributed data locations reduce the ability of the interpolation to accurately capture spatial variability. If large areas have few or no observations, the model has to extrapolate over these gaps often leading to less reliable and more uncertain estimates. Incomplete spatial coverage means key local features may be missed out. Expending the observed data in future research is recommended to enhance the robustness of the model and accuracy. This will ensure more reliable predictions and support the development of practical, data-driven strategies for sustainable tourism management in Bali.

ACKNOWLEDGEMENT
The author would like to thank the supervisors and the reviewers for their valuable efforts in providing constructive suggestions which have contributed to the improvement of this research.

REFERENCES
Adhikary, S. K., Muttil, N., & Yilmaz, A. G. (2017). Cokriging for enhanced spatial interpolation of rainfall in two Australian catchments. *Hydrological Processes*, *31*(12), 2143–2161. https://doi.org/10.1002/hyp.11163
Amelia, R., Julianti, E., & Guskarnali. (2023). Implementation of Inverse Distance Weighting (IDW) and Kriging method for distribution pattern humidity and temperature data on weather changes in the Bangka Islands. *IOP Conference Series: Earth and Environmental Science*, *1267*(1), 012091. https://doi.org/10.1088/1755-1315/1267/1/012091
Ananta, M. I., Limantara, L. M., & Soetopo, W. (2024). The Impact of Climate Change on Air Temperature in the Rainy and Dry Seasons in East Java, Indonesia: A Case Study of Climate Change in the Wlingi Dam Area. *International Journal of Environmental Impacts*, *7*(2), 169–180. https://doi.org/10.18280/ijei.070202
Atasoy, M., & Guneysu Atasoy, F. (2020). The Impact of Climate Change on Tourism: A Causality Analysis. *Turkish Journal of Agriculture - Food Science and Technology*, *8*(2), 515–519. https://doi.org/10.24925/turjaf.v8i2.515-519.3250
Bachrudin, A., Ruchjana, B. N., Abdullah, A. S., & Budiarto, R. (2023). Spatio-Temporal Model of a Product–Sum Simulation on Stream Network Based on Hydrologic Distance. *Water*, *15*(11), 2039. https://doi.org/10.3390/w15112039
Baldwin, J. W., Benmarhnia, T., Ebi, K. L., Jay, O., Lutsko, N. J., & Vanos, J. K. (2023). Humidity's Role in Heat-Related Health Outcomes: A Heated Debate. *Environmental Health Perspectives*, *131*(5). https://doi.org/10.1289/ehp11807
Das, P., & Barman, S. (2025). Perspective Chapter: An Overview of Time Series Decomposition and Its Applications. In *Applied and Theoretical Econometrics and Financial Crises [Working Title]*. IntechOpen. https://doi.org/10.5772/intechopen.1009268
Dhaher, G., & Shexo, A. (2023). Using Kriging Technique to Interpolate and Forecasting Temperatures Spatio-Temporal Data. *European Journal of Pure and Applied Mathematics*, *16*(1), 373–385. https://doi.org/10.29020/nybg.ejpam.v16i1.4613
Ding, Q., Wang, Y., Zheng, Y., Wang, F., Zhou, S., Pan, D., Xiong, Y., & Zhang, Y. (2024). Subsurface Geological Profile Interpolation Using a Fractional Kriging Method Enhanced by Random Forest Regression. *Fractal and Fractional*, *8*(12), 717. https://doi.org/10.3390/fractalfract8120717
Du, Z., Wu, S., Kwan, M.-P., Zhang, C., Zhang, F., & Liu, R. (2018). A spatiotemporal regression-kriging model for space-time interpolation: A case study of chlorophyll-a prediction in the coastal areas of Zhejiang, China. *International Journal of Geographical Information Science*, *32*(10), 1927–1947. https://doi.org/10.1080/13658816.2018.1471607
Jong, M.-C., Puah, C.-H., & Arip, M. A. (2024). The Impact of Climate Change on Tourism Demand in China. *International Journal of Energy Economics and Policy*, *14*(3), 482–488. https://doi.org/10.32479/ijeep.14149
Khan, M., Almazah, M. M. A., EIlahi, A., Niaz, R., Al-Rezami, A. Y., & Zaman, B. (2023). Spatial interpolation of water quality index based on Ordinary kriging and Universal kriging.

Geomatics, Natural Hazards and Risk, *14*(1), 2190853. https://doi.org/10.1080/19475705.2023.2190853

Krock, M., Bessac, J., Stein, M. L., & Monahan, A. H. (2022). Nonstationary seasonal model for daily mean temperature distribution bridging bulk and tails. *Weather and Climate Extremes*, *36*, 100438. https://doi.org/10.1016/j.wace.2022.100438

Lambardi Di San Miniato, M., Bellio, R., Grassetti, L., & Vidoni, P. (2022). Separable spatio-temporal kriging for fast virtual sensing. *Applied Stochastic Models in Business and Industry*, *38*(5), 806–829. https://doi.org/10.1002/asmb.2697

Li, S., Griffith, D. A., & Shu, H. (2020). Temperature prediction based on a space–time regression-kriging model. *Journal of Applied Statistics*, *47*(7), 1168–1190. https://doi.org/10.1080/02664763.2019.1671962

Liu, D. (2024). The prediction and analysis of global climate change based on SARIMA. *Applied and Computational Engineering*, *40*(1), 268–273. https://doi.org/10.54254/2755-2721/40/20230665

Lukić, D., Petrović, M. D., Radovanović, M. M., & Tretiakova, T. N. (2021). The role of TCI and TCCI indexes in regional tourism planning. *European Journal of Geography*, *12*(4), 6–15. https://doi.org/10.48088/ejg.d.luk.12.4.006.015

Lv, J., & Du, S. (2021). Kriging Method-Based Return Prediction of Waste Electrical and Electronic Equipment in Reverse Logistics. *Applied Sciences*, *11*(8), 3536. https://doi.org/10.3390/app11083536

Mondal, S. K., Ahmmad, M. S., Khan, S., Chowdhury, M. H., Paul, G. K., Binyamin, Md., Gupta, P. S., Purohit, S., & Chakrabortty, R. (2025). Modeling and Forecasting Monthly Humidity in South Asia: A SARIMA Approach. *Earth Systems and Environment*. https://doi.org/10.1007/s41748-025-00607-0

O'Rourke, S., & Kelly, G. E. (2015). Spatio-temporal Modelling of Forest Growth Spanning 50 Years – The Effects of Different Thinning Strategies. *Procedia Environmental Sciences*, *26*, 101–104. https://doi.org/10.1016/j.proenv.2015.05.008

Rahmawati, N. (2020). Space-time variogram for daily rainfall estimates using rain gauges and satellite data in mountainous tropical Island of Bali, Indonesia (Preliminary Study). *Journal of Hydrology*, *590*, 125177. https://doi.org/10.1016/j.jhydrol.2020.125177

Ramadhani, D. P., Alamsyah, A., Febrianta, M. Y., & Damayanti, L. Z. A. (2024). Exploring Tourists' Behavioral Patterns in Bali's Top-Rated Destinations: Perception and Mobility. *Journal of Theoretical and Applied Electronic Commerce Research*, *19*(2), 743–773. https://doi.org/10.3390/jtaer19020040

Ro, Y., & Yoo, C. (2022). Numerical Experiments Applying Simple Kriging to Intermittent and Log-Normal Data. *Water*, *14*(9), 1364. https://doi.org/10.3390/w14091364

Simorangkir, C. O., Ramadhan, G., Sukran, M. A., & Manalu, T. (2024). Tourism Development Impact on Economic Growth and Poverty Alleviation in West Java. *Jurnal Kepariwisataan Indonesia: Jurnal Penelitian Dan Pengembangan Kepariwisataan Indonesia*, *18*(2), 175–196. https://doi.org/10.47608/jki.v18i22024.175-196

Susanto, J., Zheng, X., Liu, Y., & Wang, C. (2020). The Impacts of Climate Variables and Climate-Related Extreme Events on Island Country's Tourism: Evidence from Indonesia. *Journal of Cleaner Production*, *276*, 124204. https://doi.org/10.1016/j.jclepro.2020.124204

Taharin, M. R., & Roslee, R. (2021). The Application of Semi Variogram and Ordinary Kriging in Determining the Cohesion and Clay Percentage Distribution in Hilly Area of Sabah, Malaysia. *International Journal of Design & Nature and Ecodynamics*, *16*(5), 525–530. https://doi.org/10.18280/ijdne.160506

Toersilowati, L., Siswanto, B., Maryadi, E., Susanti, I., Suhermat, M., Witono, A., Sipayung, S. B., Rahayu, S. A., 'Adany, F., Aminuddin, J., & Lubis, R. F. (2022). The Projections of Climate Change using Conformal Cubic Atmospheric Model (CCAM) in Bali—Indonesia. *IOP*

Conference Series: Earth and Environmental Science, *1047*(1), 012033. https://doi.org/10.1088/1755-1315/1047/1/012033

Venkatachalam, P., & Kumar, M. (2017). Space-Time Variogram Modeling. In S. Shekhar, H. Xiong, & X. Zhou (Eds.), *Encyclopedia of GIS* (pp. 1932–1938). Springer International Publishing. https://doi.org/10.1007/978-3-319-17885-1_1643

Zaharieva, S., Georgiev, I., Georgiev, S., Borodzhieva, A., & Todorov, V. (2025). A Method for Forecasting Indoor Relative Humidity for Improving Comfort Conditions and Quality of Life. *Atmosphere*, *16*(3), 315. https://doi.org/10.3390/atmos16030315

Zeiss, H., Graw, K., & Matzarakis, A. (2022). Impact of the Destination Weather Conditions on Decision and Complaint Behavior of Guests Who Booked Vacation Rentals. *Atmosphere*, *13*(12), 1998. https://doi.org/10.3390/atmos13121998

Zeng, Y., Filimonau, V., Wang, L., & Zhong, L. (2023). The impact of perceived unfavorable weather on tourist loyalty in high-altitude destinations: The case of the Qinghai-Tibet plateau, China. *Journal of Outdoor Recreation and Tourism*, *43*, 100658. https://doi.org/10.1016/j.jort.2023.100658

Zhao, J., Li, C., Yang, T., Tang, Y., Yin, Y., Luan, X., & Sun, S. (2020). Estimation of high spatiotemporal resolution actual evapotranspiration by combining the SWH model with the METRIC model. *Journal of Hydrology*, *586*, 124883. https://doi.org/10.1016/j.jhydrol.2020.124883